

# Interest Points Localization for Brain Image Using Landmark-Annotated Atlas

Huanxiang Lu, Lutz-Peter Nolte, Mauricio Reyes

Institute for Surgical Technology and Biomechanics, University of Bern, Bern, Switzerland

Received 30 January 2012; revised 22 March 2012; accepted 4 April 2012

**ABSTRACT:** The localization of clinically important points in brain images is crucial for many neurological studies. Conventional manual landmark annotation requires expertise and is often time-consuming. In this work, we propose an automatic approach for interest point localization in brain image using landmark-annotated atlas (LAA). The landmark detection procedure is formulated as a problem of finding corresponding points of the atlas. The LAA is constructed from a set of brain images with clinically relevant landmarks annotated. It provides not only the spatial information of the interest points of the brain but also the optimal features for landmark detection through a learning process. Evaluation was performed on 3D magnetic resonance (MR) data using cross-validation. Obtained results demonstrate that the proposed method achieves the accuracy of  $\sim 2$  mm, which outperforms the traditional methods such as block matching technique and direct image registration. © 2012 Wiley Periodicals, Inc. *Int J Imaging Syst Technol*, 22, 145–152, 2012; Published online in Wiley Online Library (wileyonlinelibrary.com). DOI 10.1002/ima.22015

**Key words:** landmarks localization; atlas construction; Gabor filter; feature selection

## I. INTRODUCTION

In neurological studies, finding interest points that are clinically relevant in brain images is an important task for many applications such as morphological analysis and statistical shape model (Lao et al., 2004). Besides, it can also provide useful information for image processing method (e.g., seed points for segmentation, guidance for registration, etc.). However, traditional localization of landmarks is done manually. This requires expertise in brain anatomy and is usually time-consuming. It also suffers from the inconsistency from different raters (Gartus et al., 2007).

In previous works, different automatic landmark detection approaches have been proposed. In general, they can be classified into three main categories: Geometric-based, model-based, and learning-based methods.

Geometric-based methods find geometrically salient points, curvatures or surfaces to represent prominent locations in the anatomy. Note that although many point detectors are commonly used in

computer vision such as scale-invariant feature transform (Lowe, 1996), they cannot be easily extended into 3D hence not applicable for many medical images. Therefore, 3D differential operators (Thirion, 1996; Rohr, 1997) are proposed to detect interest points on the geometrical curvatures in volumetric images. Despite the computational efficiency achieved by these approaches, they are usually sensitive to image noise and do not necessarily represent the anatomically important points defined by the experts.

Model-based methods overcome the limitations of geometric-based techniques by detecting landmarks through fitting a template or a model into the input image. Some efforts have been done to detect tip-like, saddle-like, or sphere-like structure landmarks using deformable templates or 3D parametric intensity models (Frantz et al., 2000; Worz and Rohr, 2006). Whereas this approach is able to localize the predefined anatomically important points in brain images, it usually requires fine-tuned parameters for the models. For each specific landmark, the intensity distribution and the curvature parameters of the model should be well-defined independently to each other.

Recently learning-based methods attract more attentions due to its generality and versatility. In (Izard et al., 2006), the authors used a probability intensity model of three landmarks in hippocampus based on the deformation of tissue probability maps. The estimation the landmark location is equivalent to finding the best deformation from the tissue probability map to the image by likelihood maximization. A regression method was proposed by Zhou et al. (2005), in which the landmark localization is generalized as an image-based regression problem. The regressor, which infers the spatial locations of the landmarks associated with the input image, is learned using boosting method. However, the training process of this method requires large number of weak regressors to converge, resulting in large computation time. Guerrero et al. (2011) exploited a manifold learning approach based on Laplacian Eigenmaps. The position of the patches is learned in the manifold and can be used to predict the location of the landmarks via regression. Although accurate results are achieved, manifold learning usually needs large training samples, limiting the applicability of this method.

In this work, we introduce a novel method by combining the advantages of both model-based and learning-based approaches, in which a model of anatomical landmarks is created with optimal features selected from a learning process for landmark localization.

Correspondence to: Huanxiang Lu; e-mail: huanxiang.lu@istb.unibe.ch  
Grant sponsor: This work is funded by the research grant from Swiss National Science Foundation 205321 135361/1.

Consequently, interest point localization in brain images is achieved via landmark-annotated atlas (LAA). LAA is an atlas constructed from a set of brain images with anatomically important landmarks annotated. Thus, the landmark localization problem can be formulated as finding corresponding points of LAA in the input image. For each landmark, its position in the input image is detected by using a matching criteria—mutual saliency proposed by Ou et al. (2011). Different from the way that mutual saliency is used in (Ou et al., 2010), in this work a set of Gabor attributes (Manjunath and Ma, 1996) is learned for each specific anatomical landmark instead of being learned for all voxels from the training samples. In addition, a spatial prior is also modeled to facilitate the landmark localization procedure.

The structure of this article is organized as follows. First, the methodology of the framework is elaborated in Section II including the details of atlas construction, feature selection, and experiment setup. In Section III, we present the results obtained from our method on clinical datasets and compare with block matching technique and image registration. The discussion will be presented in Section IV.

## II. METHODS

As briefly introduced above, the landmark localization contains two major steps. As shown in Figure 1, the first step is to build the LAA. It consists of an average brain image with important landmarks annotated, on which optimal features are learned from a set of 48 Gabor attributes. In the second step, the positions of the landmarks in the input image can be localized using these learned features combining with a spatial prior. The following describes each step in detail.

### A. LAA Construction

**A.1. Brain Atlas Image.** LAA consists of a set of anatomically important landmarks on an average brain images. The key parts of building such atlas are creating a mean image and the landmark annotation.

To obtain the mean image, we follow the scheme proposed by Guimond et al. (2001). Given a reference image  $I_R$ , which is arbitrarily selected from the training data, and a set of  $N$  images  $I_1, \dots, I_N$  representing the group of subjects under consideration. The average image construction can be divided into the following steps:

The first step regards the evaluation of global shape differences between the reference and each image of the set. This is achieved by registering each image  $I_i$  to  $I_R$  using the novel symmetric diffeomorphic registration approach described in (Vercauteren et al., 2009). Note that, mean intensity model is not considered in this work because all images are pre-processed with the intensity histogram matching and normalized into gray scale of [0, 255]. This registration framework optimizes the update field in the log-domain to ensure the invertibility and provides stationary velocity fields as the results. These velocity fields  $V_i$  can be looked at as generators for diffeomorphic deformations through the group exponential map that can be computed using the scaling and squaring method (Arsigny et al., 2006).

The second step computes the average velocity field. Thanks to the log-Euclidean framework (Arsigny et al., 2006), statistics of the deformation, e.g., averages, can be easily computed while preserving the diffeomorphism. In the log-Euclidean framework, velocity fields are regular elements in a vector space; this allows us to use simple Euclidean arithmetic instead of more complex nonlinear techniques (Beg et al., 2005). The average velocity field is then simply computed as:

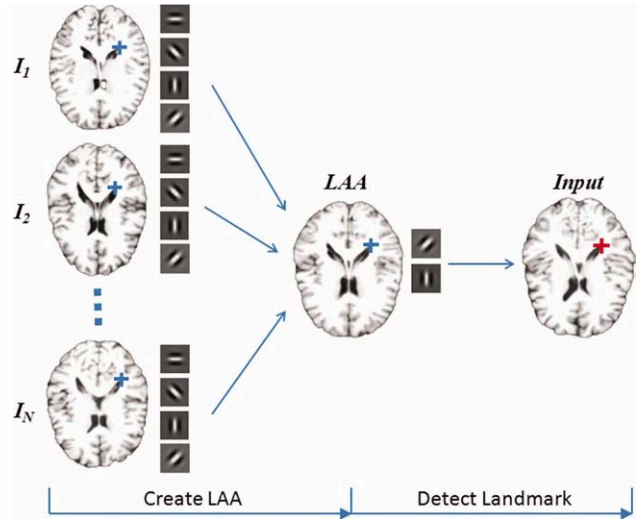


**Figure 1.** Scheme of the proposed landmark detection algorithm. The first step is to create the LAA, which is the average brain from the training samples with important landmarks annotated and best features learned. Then the spatial positions of the landmarks in the input image can be localized using these learned features. [Color figure can be viewed in the online issue, which is available at [wileyonlinelibrary.com](http://wileyonlinelibrary.com).]

$$\bar{V} = \frac{1}{N} \sum_{i=1}^N V_i \quad (1)$$

In the third step, the mean image is created by warping  $I_R$  using the mean transformation computed from the velocity field. This diffeomorphic transformation can be mapped from velocity field through an exponential operator.

$$\bar{I} = I_R \circ \exp(\bar{V}) \quad (2)$$

In total, 15 anatomical landmarks are then annotated on the mean image on different regions, including points at four tips of the ventricle, splenium of corpus callosum, genu of corpus callosum (GCC), frontal lobe cortex, anterior commissure, posterior commissure, left and right tip of putamen (L-P, R-P), center of cerebellum, fourth ventricle (FV), superior and inferior aspect of pons. These landmarks define the stable anatomical structures and can be used for brain morphometric analysis (DeQuardo et al., 1999).

**A.2. Feature Selection.** With the landmark atlases established, we adopt Gabor attributes-based mutual saliency used in DRAMMS algorithm (Ou et al., 2010) as the feature for landmark localization. The mutual saliency measures the distinctiveness of the similarity between two voxels. In other word, it calculates whether two voxels are similar to each other and not similar to any other voxels in the neighborhood. The mutual-saliency between two voxels  $p$  and  $q$ , denoted as  $ms(p, q)$ , is computed through dividing the mean similarity in the central part of the neighborhood of  $q$  [denoted as  $CN(q)$ ] by the mean similarity in the peripheral neighborhood of  $q$  [denoted as  $PN(q)$ ].

$$ms(p, q) = \frac{\frac{1}{CN(q)} \sum_{q' \in CN(q)} \text{sim}(p, q')}{\frac{1}{PN(q)} \sum_{q' \in PN(q)} \text{sim}(p, q')} \quad (3)$$

In practice,  $CN$  and  $PN$  are concentric circles around the voxel  $q$ .  $PN$  is the outer circle of  $CN$ . In Eq. (3),  $\text{sim}(p, q')$  measures the

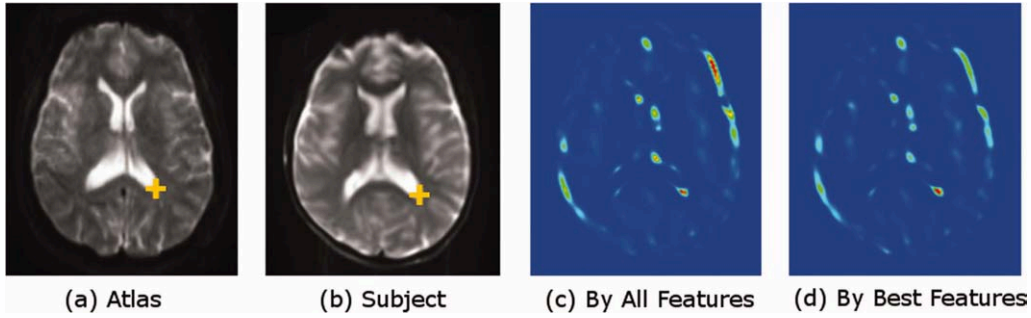


**Figure 2.** The similarities between the yellow cross in (a) atlas and (b) subject show that using learned best features (d) gives higher distinctiveness in matching points than using all Gabor features (c). The red color indicates high similarity value whereas blue means low value. [Color figure can be viewed in the online issue, which is available at [wileyonlinelibrary.com](http://wileyonlinelibrary.com).]

similarity between  $p$  and  $q'$  based on a  $D$  dimensional feature vector  $A^*$ , defined as:

$$\text{sim}(p, q') = \frac{1}{1 + \frac{1}{D} \|A^*(p) - A^*(q')\|^2} \quad (4)$$

The feature vector  $A^*$  consists of a set of 3D Gabor attributes (See Appendix A), which have been proven to be a robust and powerful tool for landmark localization in both general computer vision and medical image processing (Zhan et al., 2006). The motivation of using multiple Gabor attributes is that the multiscales and multi-orientations of the Gabor responses make it possible to characterize the image content with different dominant sizes and orientations from even noisy images. Moreover, it renders the landmark distinctive and identifiable, hence reducing the ambiguity in matching.

However, in practice, each landmark in different regions is only dominated by a few attributes (i.e., it has significant responses only with certain scales and orientations). This redundancy of the attributes reduces the uniqueness of landmark localization (Wu et al., 2007) and the computational performance. Therefore, seeking optimal features is highly necessary for the sake of accuracy and efficiency.

Consequently, we apply a learning process to find the optimal features for each anatomical landmark  $p$  annotated in the atlas. This is achieved by searching a subset attributes  $A^*$  of the total Gabor attributes  $\tilde{A}$ , which maximizes the cost function  $\text{ms}(\cdot, \cdot) \times \text{sim}(\cdot, \cdot)$  on all training data  $S$ .

$$A^* = \arg \max_{A \in \tilde{A}} \sum_{I_i \in S} [\text{ms}_{I_i}(p, p') \times \text{sim}_{I_i}(p, p')] \quad (5)$$

where  $p$  is the landmark position in the atlas image and  $p'$  is the corresponding point of  $p$  in the training image  $I_i$ .

Forward inclusion and backward elimination method (Kohavi and John, 1997) is adopted to optimize the Eq. (5). The forward inclusion step, starting from zero attribute selected, includes one Gabor attribute so that the cost function increases the most compared to including other attributes at each iteration. The procedure stops until no inclusion increases the cost function value. The backward elimination step, on the other hand, starting from all attributes selected, at each iteration eliminates one Gabor attribute so that the cost function increases the most compared to excluding other attributes. The final optimal attributes  $A^*$  are the intersection between the selected attributes from forward inclusion step and backward elimination step. As illustrated in Figure 2, the distinctiveness of the matching is enhanced after the learning process. The LAA is then created once the optimal features are learned for all the anatomical landmarks annotated on the atlas image.

**B. Landmark Localization.** With the LAA established, the input image is first affinely registered to the atlas by maximizing the mutual information between the two images so that global shape difference can be removed. In addition, the spatial variation of the corresponding landmarks is reduced, resulting in smaller search range for detection.

Moreover, we model a spatial prior function for each landmark using the spatial information of the landmarks during the training process so that we can restrict the search range for each landmark to those locations which have a nonzero probability. In practice, the spatial prior probabilities of each landmark is modeled based on the position of the landmark in the training set using kernel (or Parzen window) density estimation.

Finally, the landmark localization can be formulated as finding corresponding point  $q^*$  of landmark  $p$  in the input image, which maximizes the cost function in Eq. (5) multiplied by the spatial prior  $G_p(q)$  by searching the region  $\Omega$  defined by the spatial prior:

$$q^* = \arg \max_{q \in \Omega} G_p(q) \times \text{ms}(p, q) \times \text{sim}(A^*(p), A^*(q)), \quad (6)$$

where  $G_p(q)$  is a Gaussian kernel function of the landmark position of  $p$  generated from the training samples.

**C. Experiment Setup.** To evaluate the proposed method, we obtained 10 subject T1 images from the IXI dataset (<http://www.brain-development.org/>) with dimension of  $256 \times 150 \times 256$  and voxel size of  $0.9375 \times 1.2 \times 0.9375 \text{ mm}^3$ . Due to the limited number of datasets that we possess, cross validation was performed to evaluate the algorithm. Therefore, in total 10 tests were carried out. We first manually annotated 15 landmarks on anatomically important regions on all datasets as stated in Section II. Then, in each test, nine datasets are used as training data to construct the LAAs. The landmarks positions on the atlases were then automatically computed by composing the mean transformation on the landmarks in the reference image, from which the optimal features were trained. Then the trained atlases and best features were used in the validation dataset to perform landmark detection.

We initially chose a Gabor filter bank of axial and sagittal view of the image with three different scales and four orientations in both real and imaginary domain, hence in total 48 Gabor attributes. After feature selection, the number of features reduces around less than 20 depending on different landmarks.

We compared our algorithm to two other methods: block-matching (Jordan et al., 1997), which is a classical algorithm in computer vision used for object tracking; and image registration, which is used to search point-to-point correspondences in the images. For

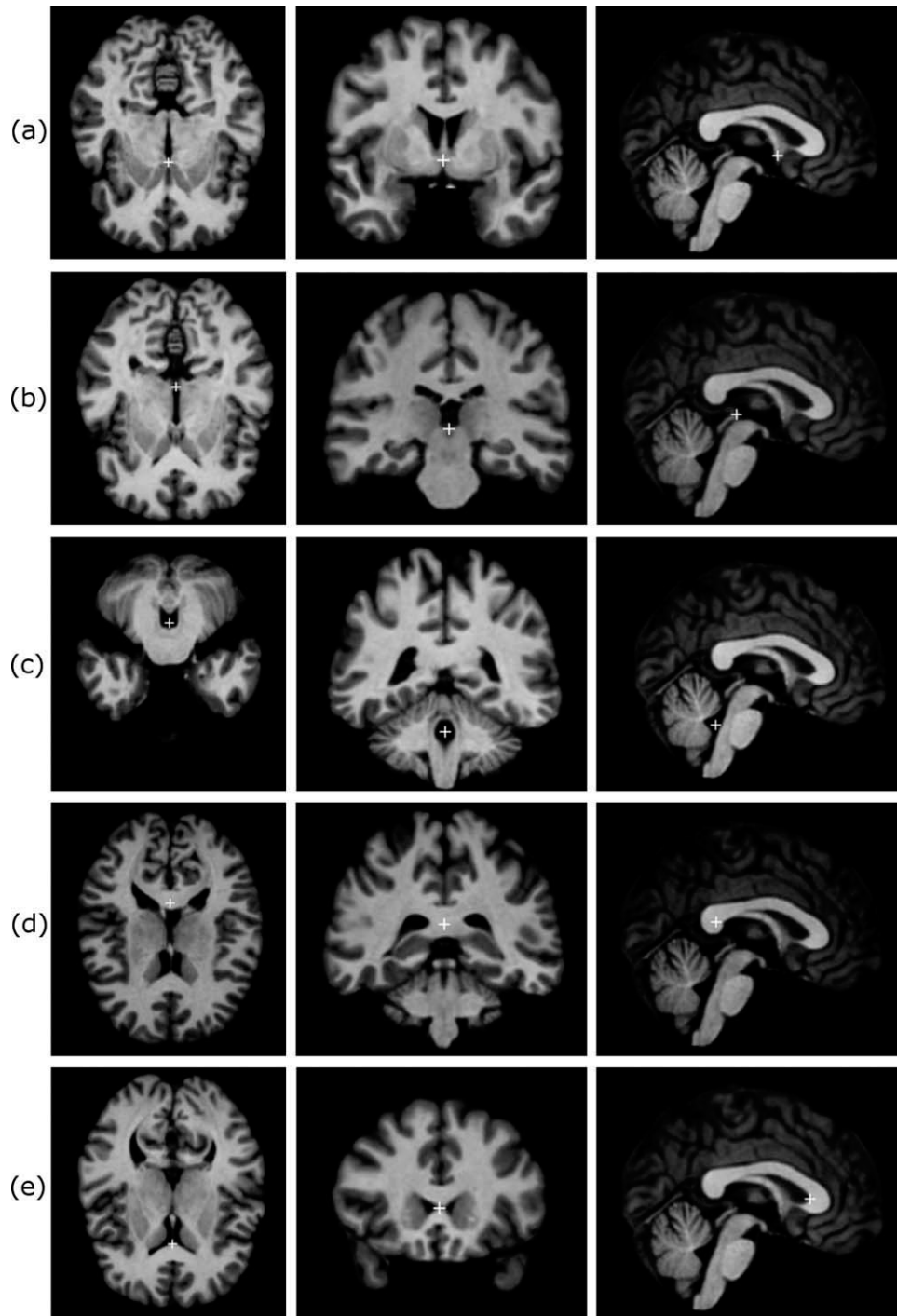


**Figure 3.** Landmark detection result on one data using the proposed method. White crosses indicate the detected points in all axial, coronal, and sagittal views. (a) anterior commissure (AC), (b) posterior commissure (PC), (c) fourth ventricle (FV), (d) splenium of corpus callosum (SCC), (e) genu of corpus callosum (GCC), (f) leftanterior tip of the ventricle, (g) right-anterior tip of the ventricle, (h) left-posterior tip of the ventricle, (i) right-posterior tip of the ventricle, (j) frontal lobe cortex (FLC), (k) left-anterior tip of putamen, (l) rightanterior tip of putamen, (m) center of cerebellum (CC), (n) superior aspect of pons (SP), and (o) inferior aspect of pons (IP).

block-matching, we used the block size of  $40 \times 40 \times 40$  and the gradient descent optimization to search the optimal position. For image registration, we adopted diffeomorphic demons algorithm with step size of 2.0 and regularization kernel size of 1.0. Multi-resolution strategy was adopted by using three different levels.

Affine registration was first applied on the input images for all the compared methods to remove the global shape difference to facilitate the landmark localization. All the methods were implemented in C++ with the help of Insight Toolkit library (<http://www.itk.org>).

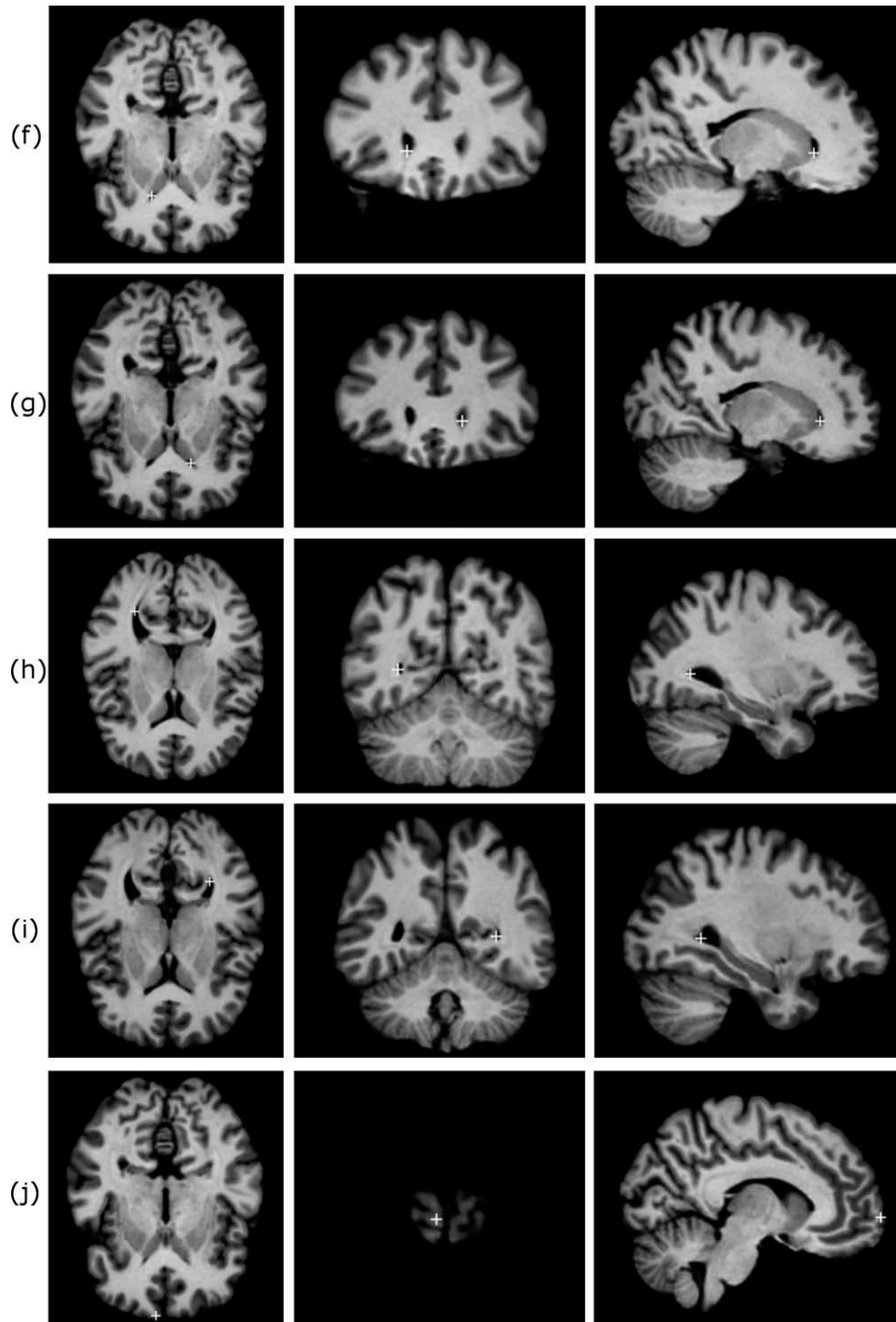


Figure 3. (Continued)

### III. RESULTS

Figure 3 shows the result of our method on one test data. Visually, all the 15 landmarks are well detected. To perform the statistical analysis, we also measured quantitatively the accuracy by computing the Euclidean distance between the detected landmark and ground truth. Table I shows the results from all three methods on all 10 datasets. The proposed LAA achieves the best accuracy for most landmarks except for FV, cerebellum, and GCC where image registration and block-

matching obtains better results. This could be due to the small number of training samples used in the experiment, which cannot cover large shape variation of the surrounding tissue of these two landmarks. Overall, LAA yields the average error of 2.12 mm whereas block-matching and registration obtains 2.66 and 2.51 mm, respectively. Statistical analysis is performed by using t-test, demonstrating the statistical difference between LAA and the other two methods ( $p = 0.0016$  with block-matching,  $p = 0.02$  with registration).

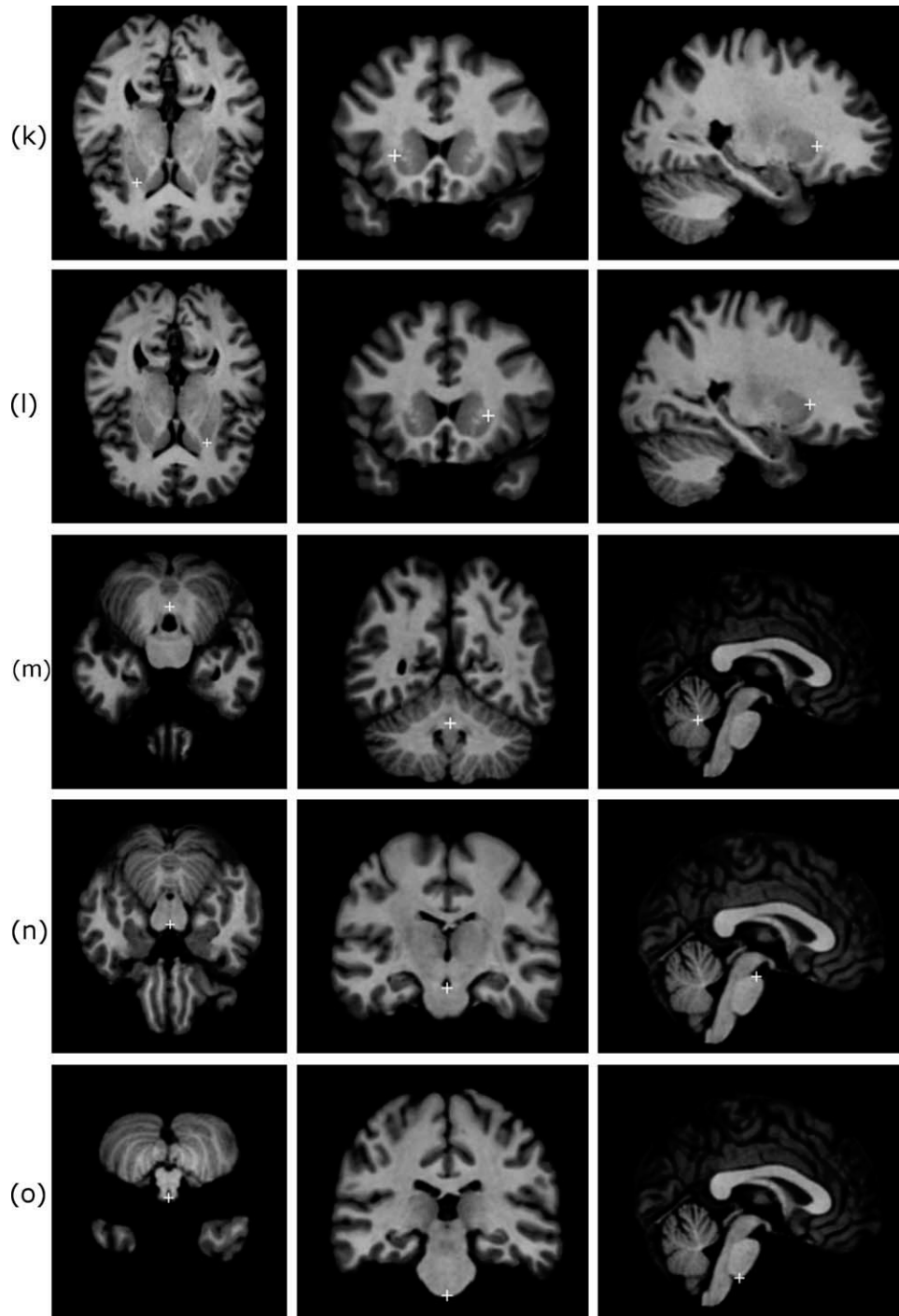


Figure 3. (Continued)

The execution time of our algorithm is about 1 min per image on an Intel Pentium PC with 3.2 GHz, running Windows XP. Block-matching approach uses only  $\sim 30$  s, whereas image registration takes more than 5 min to converge.

#### IV. DISCUSSION

In this article, we present a new approach for the localization of anatomical point landmarks in 3D brain images. LAA is introduced to formulate a problem of finding corresponding point of an atlas, in

which anatomically important landmarks are annotated. By using an optimized multiscale and multiorientation Gabor attribute vector, which increases the uniqueness of the interest point and reducing the matching ambiguity, accurate localization of the anatomical landmarks is achieved.

Similar to DRAMMS algorithm (Ou et al., 2011), we also use mutual saliency to measure the distinctiveness of the point in this work. However, there are two main differences between the ways that mutual saliency is used in the proposed method and in DRAMMS.

**Table I.** The comparison of the results from block-matching, image registration and the proposed method. The accuracy is measured by the Euclidean distance between the detected landmarks and the ground truth in millimeter

Landmark	Block Matching		Registration		LAA	
	Mean	Std	Mean	Std	Mean	Std
AC	2.380	0.841	2.082	0.720	1.891	0.832
PC	1.983	1.186	1.806	0.612	1.572	0.960
FV	2.525	1.214	1.559	0.795	2.180	0.910
SCC	2.477	2.227	4.059	2.609	1.731	0.475
GCC	1.389	0.434	2.310	0.718	1.840	0.891
TIV (L-A)	2.415	1.402	2.325	1.490	2.239	1.098
TIV (R-A)	3.076	2.390	3.002	1.760	1.917	1.384
TIV (L-P)	3.743	3.348	2.546	2.711	2.209	0.761
TIV (R-P)	3.213	3.363	2.861	3.039	2.577	1.273
Putamen (L-A)	2.932	1.336	2.909	0.904	2.416	0.790
Putamen (R-A)	2.980	1.164	2.351	1.362	2.761	0.988
FLC	3.630	1.706	3.465	2.260	2.127	0.866
Cerebellum	10128	0.734	1.744	0.855	2.494	1.095
SP	2.456	0.983	2.309	0.796	2.031	1.041
IP	2.535	1.817	2.584	1.921	1.910	0.625

1. Since DRAMMS is a general-purpose registration algorithm, the features are learned from different points with various geometrical representation uniformly scattered in the image. Contrarily, in LAA, the features are learned for each specific landmark. Thus, the optimal features are equal for all the points in the image in DRAMMS, whereas in LAA the features are specifically tailored for each different landmark.
2. Different from DRAMMS, Spatial prior is learned in the proposed method to weight the cost function and define the search region for landmark localization.

Evaluation on 3D MR brain images was performed by measuring the Euclidean distance between the detected landmarks and the ground truth. The results of the proposed LAA method are compared to the ones of block-matching technique and diffeomorphic demons algorithm. Note that although methods for localizing specific landmarks have been proposed (Worz and Rohr, 2006; Guerrero et al., 2011), the implementation of these methods are unfortunately not available for the community, nor a common database of annotated datasets is available for benchmarking. The same applies for DRAMMS, and although we agree that it is a more interesting comparison than using Demons algorithm, implementing this sophisticated algorithm requires substantial efforts that are beyond the scope of this work.

Despite limited number of training data was used due to the lack of expert-annotated brain images available in the community, obtained results from the proposed method still demonstrate significant better accuracy compared to block-matching technique and image registration technique. On the other hand, it would also be interesting for us to apply the method on larger training samples to see if the localization accuracy will be improved. Besides, the superior performance of the proposed method over image registration technique indicates that the detected landmarks can serve as prior information to guide the registration procedure (Lu et al., 2010).

For future works, it would be interesting for us to try more feature selection methods due to the variety of different learning techniques available in the computer vision and machine learning community. In addition, we would like to explore the correlation of the 15 landmarks to study the dependencies of the spatial locations.

The LAA could be combined with a graphical model or statistical appearance model to increase the robustness and computation efficiency.

## APPENDIX A. 3D GABOR ATTRIBUTES

The 3D Gabor attributes are approximated by using two banks of 2D Gabor filters located at two orthogonal planes of a 3D image. These two orthogonal planes can typically be axial and sagittal planes, from which the Gabor filter banks can be computed as:

$$\begin{aligned} g_{m,n}(x, y) &= a^{-m} g(a^{-m} x'_g, a^{-m} y'_g), \\ h_{m,n}(y, z) &= a^{-m} g(a^{-m} y'_g, a^{-m} z'_g), \end{aligned} \quad (A1)$$

where  $a = \left(\frac{U_h}{U_l}\right)^{-\frac{1}{3-1}}$  represents the scale factor with  $U_h$  and  $U_l$  being respectively the upper and lower center frequencies of interest,  $m$  is the scale index;  $x'_g = x \cos\left(\frac{n\pi}{N}\right) + y \sin\left(\frac{n\pi}{N}\right)$ ,  $y'_g = -x \sin\left(\frac{n\pi}{N}\right) + y \cos\left(\frac{n\pi}{N}\right)$ ,  $y'_h = y \cos\left(\frac{n\pi}{N}\right) + z \sin\left(\frac{n\pi}{N}\right)$ ,  $z'_h = -y \sin\left(\frac{n\pi}{N}\right) + z \cos\left(\frac{n\pi}{N}\right)$  are rotated coordinates with  $n$  being the orientation index. The respective mother functions are represented as follow:

$$\begin{aligned} g(x, y) &= \left(\frac{1}{2\pi\sigma_x\sigma_y}\right) \exp\left[-\frac{1}{2}\left(\frac{x^2}{\sigma_x^2} + \frac{y^2}{\sigma_y^2}\right) + j2\pi W_x\right], \\ h(x, y) &= \left(\frac{1}{2\pi\sigma_y\sigma_z}\right) \exp\left[-\frac{1}{2}\left(\frac{y^2}{\sigma_y^2} + \frac{z^2}{\sigma_z^2}\right) + j2\pi W_y\right], \end{aligned} \quad (A2)$$

where  $\sigma_x$ ,  $\sigma_y$ , and  $\sigma_z$  denotes the standard deviation of the Gaussian envelope,  $W_x$  and  $W_y$  are the central frequencies in each plane respectively.

## REFERENCES

- V. Arsigny, O. Commowick, X. Pennec, and N. Ayache, A Log-Euclidean framework for statistics on diffeomorphisms, In Proceedings of MICCAI, Copenhagen, Denmark (2006), 924–931.
- M.F. Beg, M.I. Miller, A. Troune, and L. Younes, Computing large deformation metric mappings via geodesic flows of diffeomorphisms, *Int J Comput Vis* 61 (2005), 139–157.
- J.R. DeQuardo, M.S. Keshavan, F.L. Bookstein, W.W. Bagwell, W.D.K. Green, J.A. Sweeny, G.L. Haas, R. Tandon, N.R. Schoolwer, and J.W. Pettegrew, Landmark-based morphometric analysis of first-episode schizophrenia, *Biol Psychiatry* 45 (1999), 1321–1328.
- S. Frantz, K. Rohr, and H.S. Stiehl, Localization of 3D anatomical point landmarks in 3D tomographic images using deformable models. In Proceedings of MICCAI, Pittsburg, USA (2000), 492–501.
- A. Gartus, A. Geissler, T. Foki, A.R. Tahamtan, G. Pahs, M. Barth, K. Pinker, S. Trattig, and R. Beisteiner, Comparison of fMRI coregistration results between human experts and software solutions in patients and healthy subjects, *Eur Radiol* 17 (2007), 1634–1643.
- R. Guerrero, R. Wolz and D. Rueckert, Laplacian Eigenmaps manifold learning for landmark localization in brain MR images, In proceedings of MICCAI, Toronto, Canada (2011), 566–573.
- A. Guimond, J. Meunier, and J.-P. Thirion, Average brain models: A convergence study. *Comput Vis Image Understand* 77 (2001), 192–210.
- C. Izard, B. Jedynak, and C.E.L. Stark, Spline-based probabilistic model for anatomical landmark detection. In proceedings of MICCAI, Copenhagen, Denmark (2006), 849–856.

- F.D. Jordan, M. Schuetz, and M. Kunt, Fast hybrid block/region-based algorithm for object tracking. In Proceedings of SPIE, Boston, USA (1997), 2915: 96–107.
- R. Kohavi and G.H. John, Wrappers for feature subset selection. *Artif Intell* 97 (1997), 273–324.
- Z. Lao, D. Shen, Z. Xue, B. Karacali, S.M. Resnick, and C. Davatzikos, Morphological classification of brains via high-dimensional shape transformations and machine learning methods, *NeuroImage* 21 (2004), 46–57.
- D.G. Lowe, Object recognition from local scale-invariant features, *Proc Int Conf Comput Vis* 2 (1999), 1150–1157.
- H. Lu, P.C. Cattin, and M. Reyes, A hybrid multimodal non-rigid registration of MR images based on diffeomorphic demons. In Proceedings of EMBC, Buenos Aires, Argentina (2010), 5951–5954.
- B.S. Manjunath and W.Y. Ma, Texture features for browsing and retrieval of image data, *IEEE Trans Pattern Anal Mach Intell* 18 (1996), 837–842.
- Y. Ou, A. Besbes, M. Bilello, M. Mansour, C. Davatzikos, and N. Paragios, Detecting mutually-salient landmark pairs with MRF regularization. In proceedings of ISBI, Rotterdam, Netherland (2010), 400–403.
- Y. Ou, A. Sotiras, N. Paragios, and C. Davatzikos, DRAMMS: Deformable registration via attribute matching and mutual-saliency weighting. *Med Image Anal* 15 (2011), 622–639.
- K. Rohr, On 3D differential operators for detecting point landmarks. *Image Vis Comput* 15 (1997), 219–233.
- J.-P. Thirion, New feature points based on geometric invariants for 3D image registration. *Int J Comput Vis* 18 (1996), 121–137.
- T. Vercauteren, X. Pennec, A. Perchant, and N. Ayache, Diffeomorphic demons: efficient non-parametric image registration. *NeuroImage* 45 (2009), S61–S72.
- S. Worz and K. Rohr, Localization of anatomical point landmarks in 3D medical images by fitting 3D parametric intensity models, *Med Image Anal* 10 (2006), 41–58.
- G. Wu, F. Qi, and D. Shen, Learning best features and deformation statistics for hierarchical registration of MR brain images. In Proceedings of IPMI, Manchester, UK (2007), 160–171.
- Y. Zhan and D. Shen, Deformatble segmentation of 3D ultrasound prostate images using statistical texture matching method. *IEEE Trans Med Imag* 25 (2006), 256–272.
- S.K. Zhou, B. Georgescu, X.S. Zhou, and D. Comaniciu, Image based regression using boosting method. In proceedings of IEEE International Conference on Computer Vision, Beijing, China (2005), 541–548.